Thin Solid Films 574 (2015) 43–51

Contents lists available at ScienceDirect

Thin Solid Films

journal homepage: www.elsevier.com/locate/tsf

High rate deposition of thin film cadmium sulphide by pulsed direct current magnetron sputtering

F. Lisco [a,*], P.M. Kaminski [a], A. Abbas [a], J.W. Bowers [a], G. Claudio [a], M. Losurdo [b], J.M. Walls [a]

[a] Centre for Renewable Energy Systems Technology (CREST), School of Electronic, Electrical and Systems Engineering, Loughborough University, Leicestershire LE11 3TU, UK
[b] Institute of Inorganic Methodologies and of Plasmas, IMIP-CNR, via Orabona 4, 70126 Bari, Italy

ARTICLE INFO

Article history:
Received 15 May 2014
Received in revised form 19 November 2014
Accepted 20 November 2014
Available online 28 November 2014

Keywords:
Cadmium sulphide
Pulsed direct-current magnetron sputtering
Scanning electron microscopy
Transmission electron microscopy
Refractive index

ABSTRACT

Cadmium Sulphide (CdS) is an important n-type semiconductor widely used as a window layer in thin film photovoltaics Copper Indium Selenide, Copper Indium Gallium (di)Selenide, Copper Zinc Tin Sulphide and Cadmium Telluride (CdTe). Cadmium Sulphide has been deposited using a number of techniques but these techniques can be slow (chemical bath deposition and Radio Frequency sputtering) or the uniformity and the control of thickness can be relatively difficult (close space sublimation). In this paper we report on the development of a process using pulsed Direct Current magnetron sputtering which allows nanometre control of thin film thickness using time only. The CdS thin films deposited in this process are highly uniform and smooth. They exhibit the preferred hexagonal structure at room temperature deposition and they have excellent optical properties. Importantly, the process is highly stable despite the use of a semi-insulating magnetron target. Moreover, the process is very fast. The deposition rate using 1.5 kW of power to a 6-inch circular magnetron was measured to be greater than 8 nm/s. This makes the process suitable for industrial deployment.

1. Introduction

Cadmium Sulphide (CdS) is an important semiconductor material widely used in thin film photovoltaics as a window layer [1,2]. Cadmium Sulphide is an n-type semiconductor with a band gap of 2.42 eV. Cadmium Sulphide exists in two crystalline phases, hexagonal wurzite and the cubic zinc-blend structure. Cadmium sulphide has a bulk refractive index (n) of 2.52 at wavelength 600 nm [3] which is well suited for its application in solar cells. The refractive index value is between the index of the absorber and the Transparent Conducting Oxide (TCO) contact, which allows light trapping by refractive index matching. Radio Frequency (RF) Sputtered CdS films with refractive index in the range of 2.25–2.51 have been reported [4,5]. Sprayed films have been reported with a refractive index of 2.12 [3] and refractive indices in the range 2.19–2.32 have been reported for vacuum evaporated CdS [3,6].

Thin film CdS has been used as a n-type material to form a heterojunction in a number of photovoltaic systems including copper indium selenide (CIS) [7], copper indium gallium (di)selenide (CIGS) [8–10], copper zinc tin sulphide (CZTS) [11,12] and cadmium telluride (CdTe) [1,13–16]. Although research is being conducted to evaluate alternatives to CdS in CIGS [7,9,10], the highest efficiency devices utilise a CdS window layer [2,8]. The CdS window layer is required to provide good transmission of light through to the absorber layer in a thin film photovoltaic (PV) stack. The material must uniformly cover the absorber to avoid shunts between the absorber and the front electrode. The deposition technique is required to allow fine control of thickness since films between 40 nm and 150 nm are usually required in solar cells. The precise thickness of the CdS layer determines the degree of light absorption. A compromise is needed between uniformity of coverage of the CdS, its thickness, and light transmission into the absorber layer.

CdS has been deposited using a number of methods including: metalorganic vapour phase epitaxy [17], chemical bath deposition [7,12], close space sublimation [13,18–20], vacuum evaporation [6,16,21], and Radio Frequency (RF) magnetron sputtering [1,22–24]. RF sputtered films can be deposited at room temperature but they usually exhibit a small grain size. Magnetron sputtering deposits dense films with uniform surface coverage avoiding pinhole formation. It also offers good control of thin film thickness. RF sputtering has been used to date since CdS is a semi-insulating material and the use of DC power leads to charge build up, arcing and process instability. Unfortunately, magnetron sputtering using RF power results in low deposition rates (for example a rate of 0.3 nm/s has been reported at 250 W [24]) and involves the use of complex matching circuits. Although suitable for research purposes, the technique is not well suited to industrial deployment. In this paper, we report on the use of pulsed DC magnetron sputtering. A previous study using pulsed DC magnetron sputtering of CdS has been reported but this work focused on the wavelength and lifetime of transient species [25]. We have developed a process using pulsed DC power that can be used to sputter thin films of CdS in process

* Corresponding author.
E-mail address: F.Lisco@lboro.ac.uk (F. Lisco).

http://dx.doi.org/10.1016/j.tsf.2014.11.065

conditions which are highly stable. The major advantage is that the process produces high deposition rates suitable for use in solar module manufacturing. These rates are over an order of magnitude faster than those obtained by RF sputtering. In common with other applications we also find that the energetics of the pulsed DC process produce favourable thin film properties and the power supply configuration avoids the need for matching circuits [26,27].

2. Experimental details

CdS thin films were deposited by pulsed DC magnetron sputtering in a 'PV Solar' sputtering system (Power Vision Ltd., Crewe UK). The system is equipped with four six-inch diameter circular magnetrons mounted vertically, with an option to replace one of the magnetrons with a plasma source for reactive sputtering. The samples are mounted vertically on a rotatable carrier, designed for 5 cm × 5 cm substrates. The target to substrate distance is typically 10 cm. During the deposition process the carrier rotates at typically 120 rpm. This provides excellent uniformity in the horizontal direction. Uniformity in the vertical direction is achieved using disposable masks mounted in front of the magnetron target. The CdS thin films were sputtered using a pulsed DC power supply (Advanced Energy Inc. Pinnacle plus, 5 kW) using argon as the working gas [28].

The CdS thin films were deposited on NSG-Pilkington Transparent Electrically Conducting (TEC15 and TEC10) Fluorine doped tin oxide (FTO) coated glass substrates. Prior to the CdS deposition, the substrates were cleaned in a two-step ultrasonic bath process consisting of a 5 min

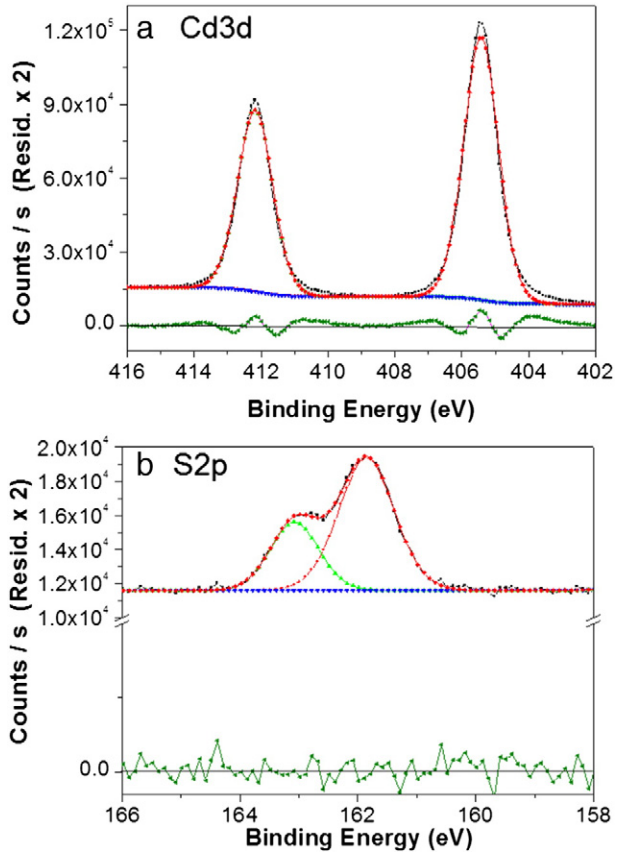

Fig. 1. The XPS spectra measured for pulsed DC deposited CdS, was not affected by the deposition conditions, showing photoelectron core levels of (a) Cd3d5/2 and Cd3d3/2 and (b) S2p for CdS thin films deposited at 10 sccm Ar, 500 W and 150 kHz. For (a) the fitting is achieved with a single Gaussian peak due to CdS and for (b) the fitting shows the splitting of S2p3/2 and S2p1/2. The green line below shows the error fitting function.

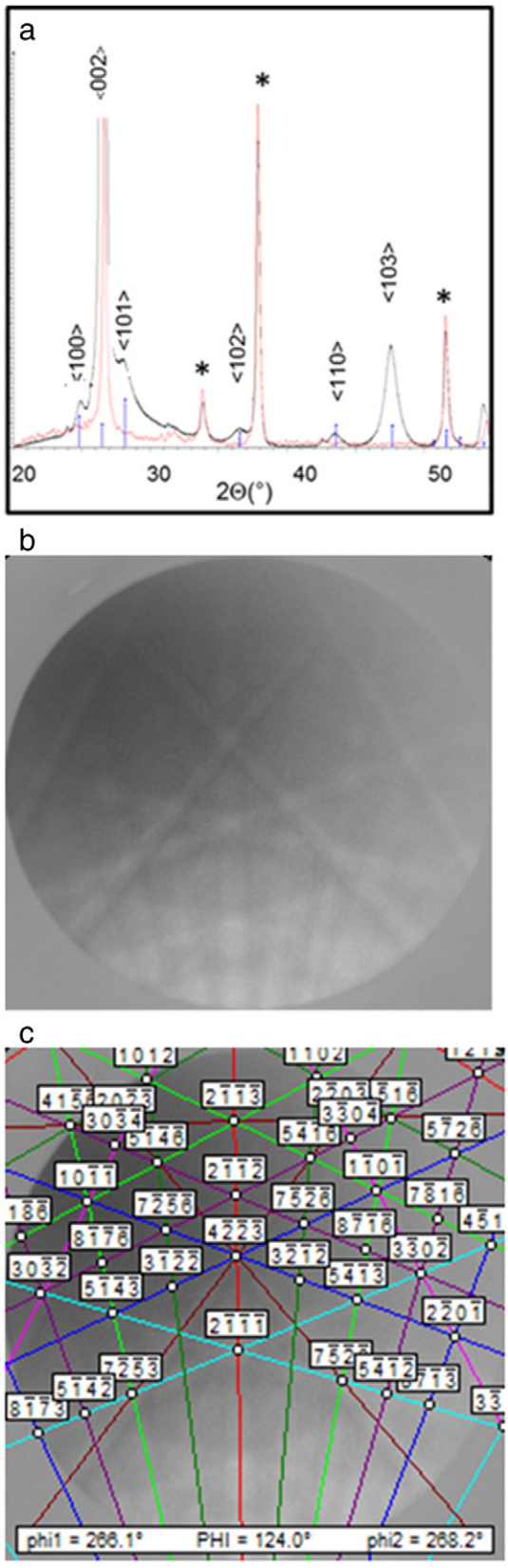

Fig. 2. (a) XRD pattern, (b) Kikuchi pattern and (c) Kikuchi phase map of a CdS film sputtered on TEC15 coated glass for 3600 s, 10 sccm Ar, 500 W, 150 kHz, 2 s (ramp time), 2 μs (reverse time). The * in (a) indicates peaks due to the TEC 15 glass substrate.

bath in a solution of Isopropanol and de-ionised water (1:10), followed by a second ultrasonic bath in de-ionised water for 5 min. Following the cleaning, the substrates were subjected to a plasma surface treatment in a mixture of 20 sccm of O_2 and 30 sccm of Ar using a plasma discharge power of 100 W and a pressure ~40 Pa to activate the surface [29,30]. The plasma treatment was carried out in a Glen100-P AE Advanced Energy system. The reactor is a parallel plate system with an AC plasma power source connected to substrate shelves which act as electrodes. The samples were then transferred to the deposition system. The chamber was evacuated to a pressure of 5×10^{-3} Pa before admitting pure Ar gas at flows in a range between 5 sccm and 20 sccm. The depositions were performed using the following process conditions: 150 kHz (pulsing frequency), 2 s (ramping time), and 1.5 μs (pulse reverse time). The effects of increasing the Ar gas flow (5 sccm, 10 sccm, 15 sccm and 20 sccm), the deposition power (250 W–1500 W) and the deposition temperature (250, 300 and 400 °C) on the film properties were investigated. At these deposition conditions, the plasma arcing was minimal during the film growth and the working pressure was measured to be 1 Pa.

The chemical composition, microstructure and optical properties of the CdS thin films were investigated. The microstructure was studied with a high resolution field emission gun scanning electron microscope (FEGSEM), Leo 1530 VP FEG-SEM, which provides the ability to visualise surface features of the material with nanometer resolution.

An X-ray Photoelectron Spectroscopy (XPS) surface analysis tool was used to obtain the chemical composition of the layers. The analysis was performed using a Thermo Scientific K-Alpha XPS. An electron flood gun was used to reduce any charging that would cause peak shifts to occur. An argon ion surface etch at 1 keV for 30 s, was carried out prior to analysis to remove surface contamination. The X-ray source used was Al K_α radiation $h\nu = 1486.6$ eV with a beam diameter of 200 microns. The High Resolution Multiplex Scan was used to evaluate the chemical state(s) of each element through its core electron binding energies. Precise determination of binding energies was made through the use of curve fitting routines applied to the peaks in the multiplex scan and sensitivity factors were taken into account to determine elemental composition. A dual beam FEI Nova 600 Nanolab was employed to prepare the transmission electron microscopy (TEM) samples. A standard in situ lift off method was used to prepare cross-sectional samples through the coating into the glass substrate. A platinum over-layer was deposited to define the surface of the samples and homogenize the final thinning of the samples. TEM images were obtained using a Jeol JEM 2000FX operating at 200 kV, with an integrated camera above the phosphor screen to obtain digital images. The TEM technique provided morphological analysis of the grain structure of the sputtered CdS films on FTO coated glass substrates. The X-ray diffraction analysis (XRD) was performed, using a Bruker D2 Phase bench-top XRD using Copper X-rays with a 1.542 nm wavelength, to investigate the crystalline structure of the material. Each sample was scanned using an angular range of 20–90° with a step size of 0.02° and a dwell time of 0.1 seconds. Electron Backscattered Diffraction (EBSD) was used for crystal analysis to measure the structure and orientation in the solid crystalline phase. Transmission Electron Back-Scatter Diffraction (t-EBSD) was used because it offers superior resolution suitable for the characterisation of the small grains of the sputtered CdS material. t-EBSD was carried out using a dual beam FEI Nova 600 equipped with an ultra-high speed Hikari, Electron backscattering diffraction (EBSD) camera, using a beam current of 6.7 nA and an acceleration voltage of 30 kV. Scanning White Light Interferometry (SWLI) (Sunstar CCI, Taylor Hobson Ltd.) was used to measure sample surface roughness and to detect the presence of pinholes. Pinholes are a known problem for thin films CdS in PV devices [28]. Pinholes are microscopic imperfections in the coating which appear as pits in the interferometer surface image. The spatial resolution of the interferometer is determined by the wavelength of light and the numerical aperture of the lens used, and is typically ~0.3 μm. The vertical resolution is typically <1 nm. The transmission, reflection and energy band gap (Eg) measurements were carried out using a spectrophotometer (Varian Cary® UV–Vis 5000). The instrument is equipped with an integrating sphere and set of gratings which allow the collection of transmission information from wavelengths in the range from 185 nm to 3.3 μm. The energy band gap E_g, was calculated as a graphic extrapolation by using the Tauc plot [31].

$$a = \frac{A\left(h\nu - E_g\right)^p}{h\nu} h\nu \tag{1}$$

with α, is the absorption coefficient A—the proportionality constant, E_g—the band gap energy, ν—the frequency, h—the Plank's constant,

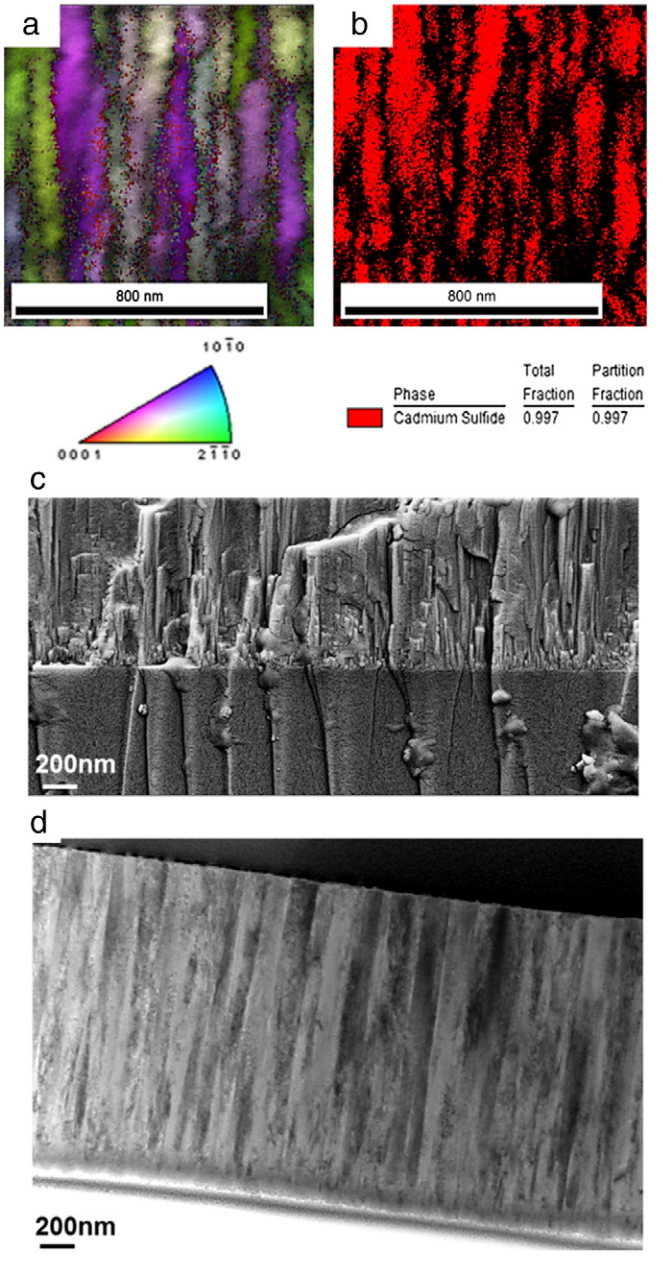

Fig. 3. (a) Transmission electron back-scatter diffraction derived map overlaid with inverse pole figure of a sputtered CdS sample. Different colours represent different orientations for grains as shown in the inverse pole figure (IPF) map. (b) Transmission electron back-scattered diffraction derived phase/confidence index map from a CdS sputtered sample; zones and the dark parts are related to the grain boundaries. (c) SEM fracture cross section of 1.6 μm thin film of CdS sputtered with 10 sccm Ar for 3600 s, 500 W. TEM image (d) of the same sample. The film shows a structure with thin columnar grains.

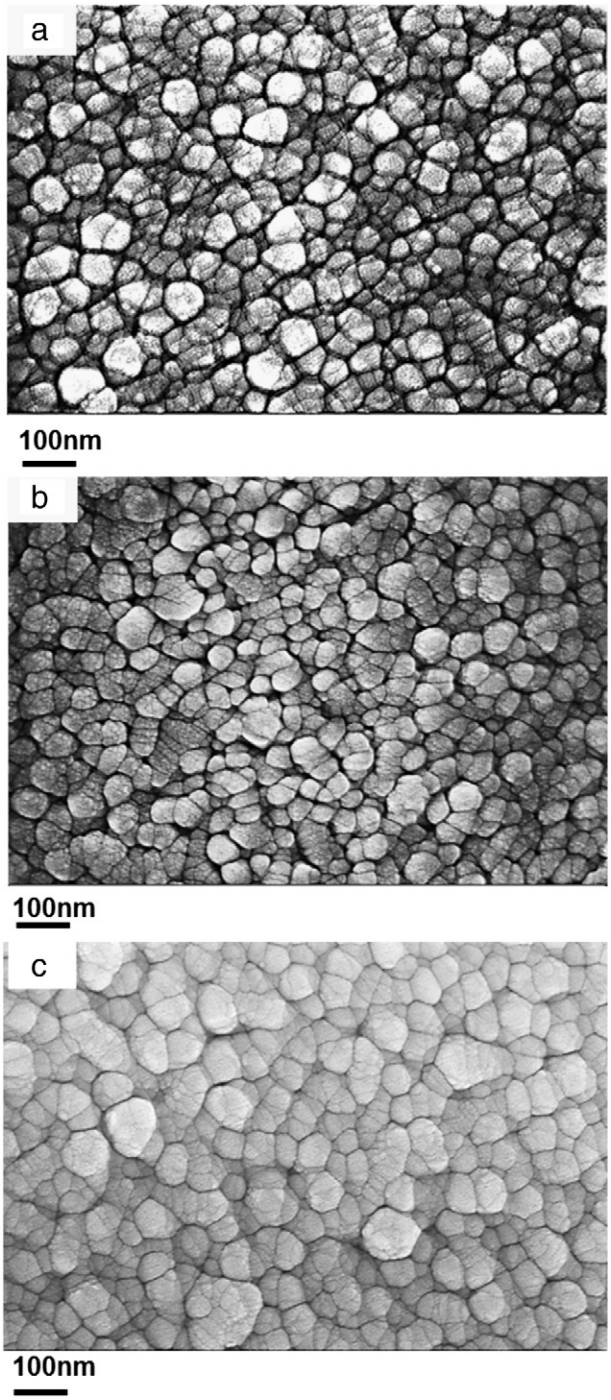

Fig. 4. SEM images of CdS films deposited at 600 s, 150 kHz, 2 s, 2.5 μs, by changing (a) the Ar gas flow from 10 sccm to (b) 20 sccm and power from 500 W to (c) 1500 W.

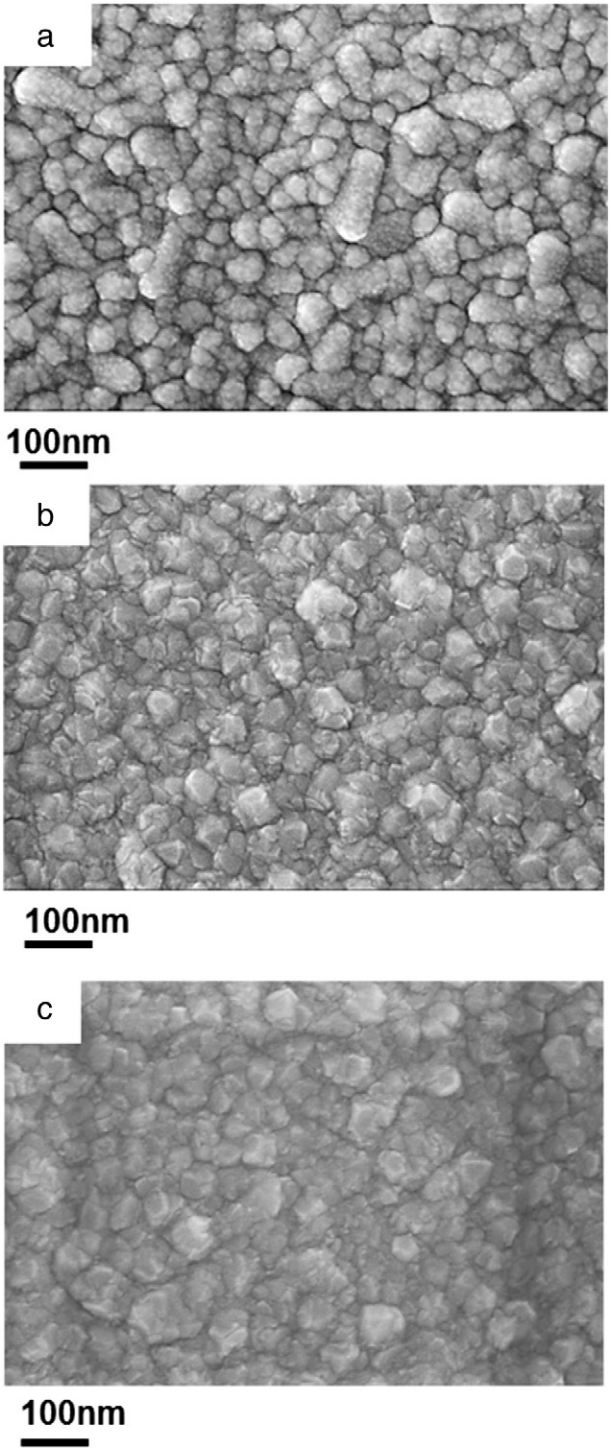

Fig. 5. SEM images of 100 nm thick CdS films, deposited at 150 kHz, 2 s, 2.5 μs, 500 W by changing the deposition temperature (a) 250 °C (b) 300 °C (c) 400 °C.

p—numerical coefficient (p = 0.5 for direct band gap material and p = 2 for indirect band gap material).

The optical properties of the thin films were also measured using spectroscopic ellipsometry (SE) (Horiba, Jobin Yvon, UVISEL); which provided information about the thickness and refractive index (and uniformity) of the deposited films. The dispersion of the real and imaginary part of the refractive index was measured in a wavelength range between 248 nm and 2100 nm. To analyse SE data and derive the energy band gap and refractive index of films, we used a three-layer model consisting of TEC-substrate/interface/CdS-film/surface-roughness/air; for the TEC substrate, the SE experimental file recorded just before starting the deposition, was used without any assumption; the interface was a Bruggeman effective medium (BEMA) [28] mixture of the top layer of the TEC substrate (SnO_2:F) and CdS; the CdS optical properties were parameterised using a double Tauc Lorentz dispersion formula [29]:

$$\varepsilon_i \begin{cases} \sum_{i=1}^{N} \frac{1}{E} \times \frac{A_i \cdot E_i \cdot C_i \cdot \left(E - E_g\right)^2}{\left(E^2 - E_i^2\right)^2 + C_i^2 \cdot E^2} & \text{for } E > E_g \\ 0 \text{ for } E \le E_g \end{cases} \quad (2)$$

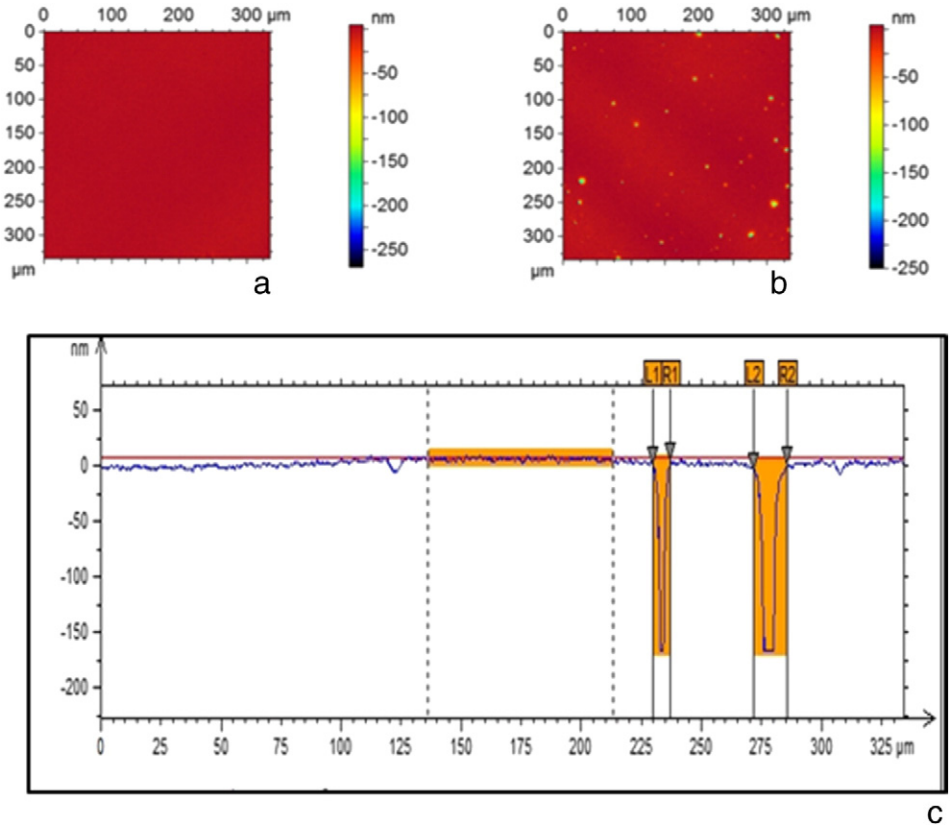

Fig. 6. SWLI surface maps of CdS films deposited at different Ar flows: 5 sccm (a) and 20 sccm (b). 2D cross section across recorded voids in the surface of CdS deposited at 20 sccm Ar flow (c). The thickness of the CdS layer was 270 nm.

where A_i, is the Tauc coefficient, E, the photon energy, E_i, the transition energy of the oscillator of highest order, C_i, the broadening term of the peak, and E_g, the optical band gap.ε_r is written as the following sum:

$$\varepsilon_r(E) = \varepsilon_r(\infty) + \sum_{i=1}^{N} \frac{2}{\pi} \cdot P \cdot \int_{E_g}^{\infty} \frac{\xi \cdot \varepsilon_i(\xi)}{\xi^2 - E^2} d\xi \quad (3)$$

The surface roughness was a BEMA mixture of 50% CdS and 50% voids. The fit parameters were the Tauc parameters and layer thicknesses.

3. Results and discussion

3.1. CdS composition, structure and morphology

Fig. 1 shows the XPS spectra of Cd3d and S2p photoelectron core levels measured for CdS films deposited at ambient temperature using different Ar gas flows. The position of the Cd peaks was 405.8 eV and 412.3 eV for $Cd3d_{5/2}$ and $Cd3d_{3/2}$ respectively; the shape and the binding energy of 161.6 eV and 162.8 eV m e a s u re d fo r $S2p_{3/2}$ and $S2p_{1/2}$ matched the theoretical values for CdS [30]. This indicated that the deposited CdS films are stoichiometric and no oxygen was incorporated into the film. This is also supported by a fitting analysis which showed only the CdS component. The XPS analysis of CdS films deposited at different values of Ar gas flow, deposition power and temperature showed that the chemical composition of the sputtered film CdS was unaffected by the deposition parameters.

Fig. 2 shows the XRD pattern measured for a CdS sputtered at ambient temperature, at an Ar flow of 10 sccm on a TEC15 glass substrate. Diffraction peaks due to the (002), (100), (101), (102), (110) and (103) reflection peaks indicate the hexagonal phase for the CdS thin film.

The hexagonal phase was also supported by t-EBSD analysis carried out on various grains. Each Kikuchi line, in the Kikuchi diffraction pattern collected in transmission electron back-scattered diffraction from a CdS grain, is associated with Bragg diffraction from one side of a single set of lattice planes and they can be labelled with the same Miller indices that are used to identify diffraction spots. Fig. 2 (b–c) shows a large number of bands overlaid with the hexagonal phase map, which provide a clear indication that each grain is of the hexagonal phase.

Additional information on the crystalline structure of individual grains was obtained by the inverse pole figure (IPF) map shown in Fig. 3. Inverse pole figure (IPF) orientation component uses a basic RGB colouring scheme, fit to an inverse pole figure. Euler angles are a set of three angles used to describe the crystallographic orientation of crystals relative to a reference co-ordinate system (usually defined by the primary SEM stage axes). Here, the value of each Euler angle is individually set to a colour scale (normally red, green, and blue), and the three are combined into a single RGB colour. Intermediate orientations are coloured by an RGB mixture of the primary components. The transmission electron back-scatter diffraction map in Fig. 3a shows that the sputtered grains have a high level of texture in the <111> direction, consistent with the XRD pattern (Fig. 2). Furthermore, the high resolution transmission electron back-scattered diffraction phase/confidence index map in Fig. 3b shows that within the grains there is a high degree of indexing, while at grain boundaries the Kikuchi pattern quality is reduced and therefore they are shown as darker regions, highlighting

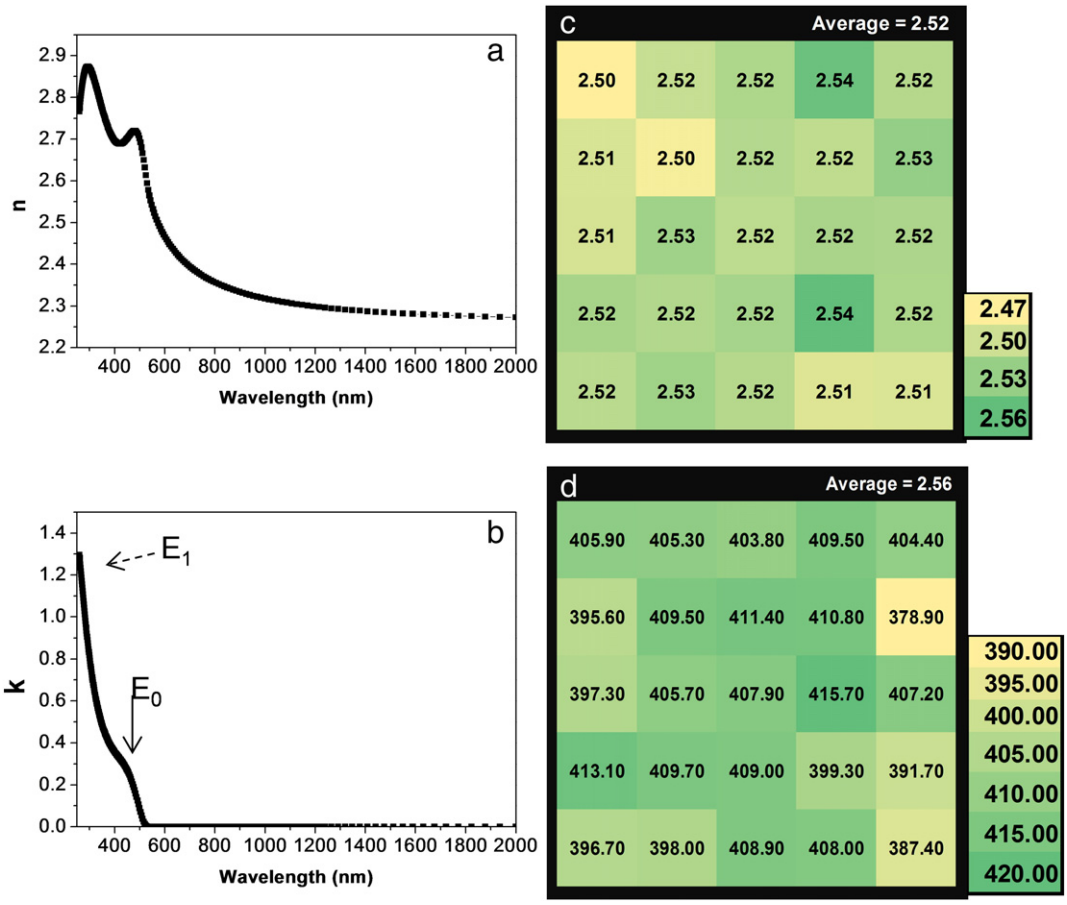

Fig. 7. Refractive index spectra of a 400 nm CdS thin film, (a) real (n) and (b) imaginary part (k), with marked E0 and E1 inter-band transition points; (c) shows map of refractive index at 550 nm, area of 5 mm × 5 mm outlined by 25 different points; (d) shows thickness map of CdS layer 400 nm thick on a 5 mm × 5 mm area outlined by 25 different points.

the columnar structure of grains, also confirmed by the TEM cross section and SEM fracture cross section images of a 1.6 μm thick CdS film deposited on TEC10 glass shown in Fig. 3c and d, respectively. The TEM image in Fig. 3d shows that the grain size is typically ~50 nm and the onset of grain coalescence is observed from the SEM surface images, shown in Figs. 4 and 5.

The SEM images in Fig. 4 show the surface morphology of the deposited CdS film, measured for films deposited at different gas flows and deposition powers. The surface morphology appeared to be mostly unaffected by the Ar gas flow and the deposition power. The substrate temperature was ambient, a few degrees above room temperature due to substrate interaction with the magnetron plasma. The thickness of each thin film was maintained at ~270 nm for this set of experiments.

Fig. 5 (a–c) shows SEM images of 100 nm thick CdS thin films deposited at different temperatures (250 °C, 300 °C and 400 °C). Increasing the deposition temperature from 250 °C to 400 °C resulted in morphology changes of the deposited CdS films. The grains of the films deposited at 250 °C appeared to have a round shape. The thin films deposited at higher temperature (300 °C and 400 °C) were more compact and showed more uniform distribution of the grain size.

Fig. 6 shows a typical surface profile obtained using SWLI for samples deposited using an Ar flow of 5 sccm and 20 sccm. The analysis showed that films deposited at Ar flows below 20 sccm had a smooth uniform surface, but when the Ar flow was increased to 20 sccm voids appeared in the SWLI image of the film surface. The voids appear as deep pits in the surface; a 2D cross section across recorded voids shows that the detected pinholes were 174 nm deep. The thin film was 270 nm thick; therefore, these pits were voids in the deposited film but no pinholes were detected.

3.2. Optical properties of the deposited CdS films

Fig. 7 shows the derived optical properties of the CdS film deposited at 10 sccm of Ar flow and 500 W deposition time for 600 s. The peak at 2.7 eV is the E_0 inter-band transition [32] in good agreement with the absorption edge of hexagonal CdS [31], while the E_1 inter-band transition at 4.9 eV is at the end of the experimental measurement range. The uniformity of the optical properties and thickness of deposited

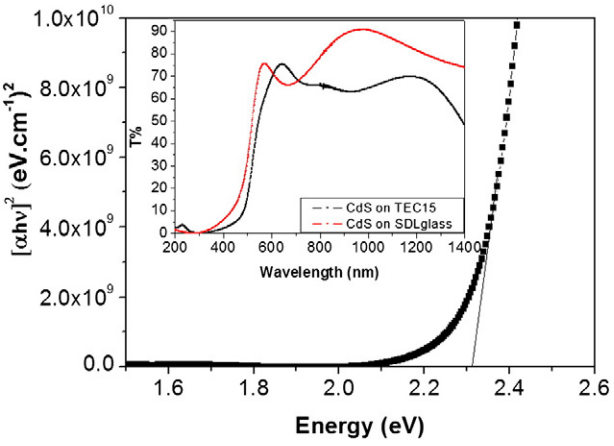

Fig. 8. Energy band gap, 2.31 eV and transmittance curve, as inset, for CdS film deposited at 600 s, 500 W, 150 kHz, 2 s, 2.5 μs with 10 sccm of Ar on TEC15 and soda lime glass.

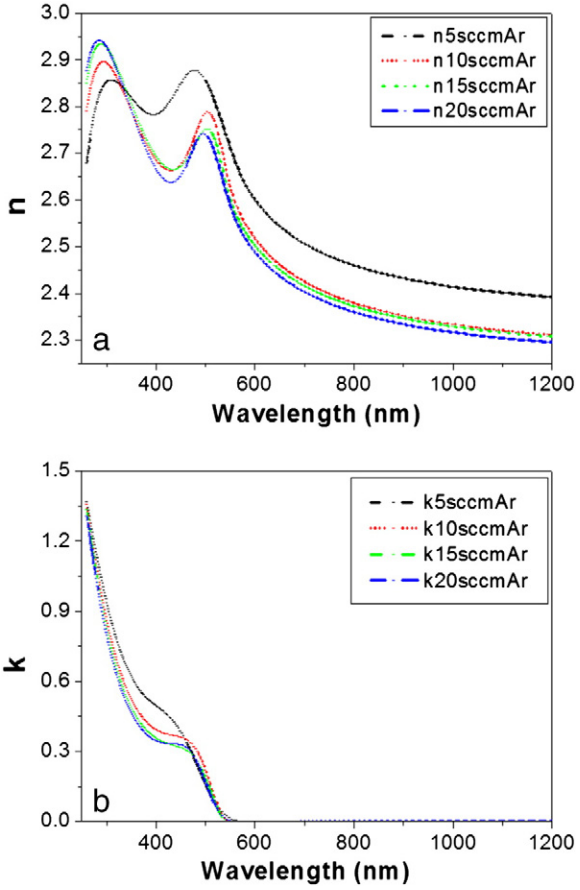

Fig. 9. (a) Refractive index, *n*; (b) extinction coefficient, *k*. For thin film CdS deposited using different argon gas flows.

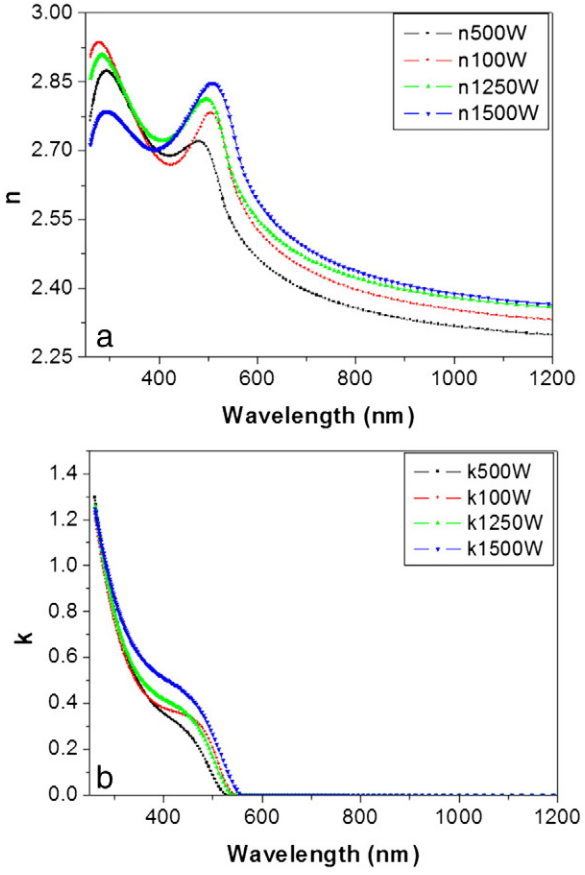

Fig. 10. Refractive index (a) and extinction coefficient (b) of CdS films sputtered at different deposition powers: 500, 1000, 1250 and 1500 W.

films was verified by ellipsometric mapping; Fig. 7 shows the distribution of the refractive index (c) and thickness (d) on a 5 mm × 5 mm area. Typically the refractive index changed in the range of 2.50–2.54, with a standard deviation of $\sigma < 0.01$.

The transmittance of this film reaches a maximum of ~80% and decreases to 0% near the absorption edge at 500 nm (Fig. 8). From the Tauc plot, an energy band gap (E_g) of 2.31 eV has been determined.

Fig. 9 shows refractive index, extinction coefficient, and transmittance measured for films deposited at different gas flows. The measurement showed that, while the extinction coefficient and band gap do not change significantly, the increase in the gas flow resulted in a lower refractive index. This is consistent with the SWLI results where for higher Ar flows, voids were present in the surface of the CdS films. Voids are known to reduce refractive index of material because the optical density is affected by the presence of these defects of the material. Consequently, the transmittance changed slightly in the range of 75%–80%. Fig. 10 shows that the deposition power affected the refractive index of films, as shown by the spectra for CdS films deposited at 5 sccm Ar flow at different deposition powers of 500, 1000, 1250 and 1500 W.

3.3. The effect of deposition parameters on the deposition rate

The influence of deposition power and gas flow on the deposition rate was studied. The results are shown in Figs. 11 and 12. The deposition rate increased linearly with the deposition power. The deposition rate was affected by the argon flow rate and working gas pressure with rate increasing from 4.26 nm/s at a flow rate of 5 sccm to 5.33 nm/s at 20 sccm, as shown in the inset. The deposition rate was observed to decrease once the argon gas flow rate was higher than 20 sccm possibly caused by scattering. The effect of changing the gas flow rate was investigated in the range between 5 and 20 sccm. The effect of substrate temperature on the deposition rate was also investigated. Fig. 13 shows the measured deposition rates for different substrate temperatures up to 400 °C. The deposition rate decreased with increasing substrate temperature [33].

4. Discussion

Thin film CdS is an important component of several thin film photovoltaic device systems including thin film CdTe, CIS, CIGS and CZTS. It is used as an n-type window layer to form the device heterojunction. Layers of thin film CdS are often deposited using a chemical bath method but this process is slow and is prone to the formation of

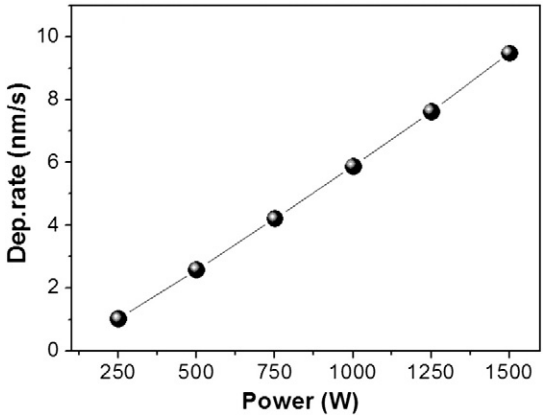

Fig. 11. Deposition rate as a function of deposition power (150 kHz, 10 sccm Ar).

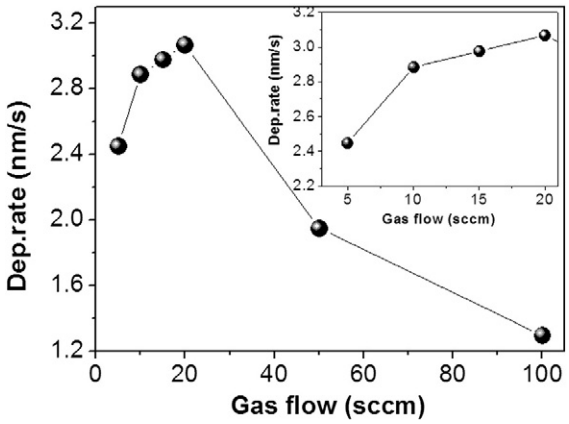

Fig. 12. Deposition rate as a function of argon gas flow at 500 W deposition power.

pinholes. The use of RF sputtering has also been widely reported but this process also suffers from low deposition rates and involves the use of complex matching circuitry. In this paper we report on the use of pulsed DC magnetron sputtering to deposit thin film CdS. Importantly, the use of pulsed DC at 150 kHz frequency results in a highly stable process with no plasma arcing. It allows close control of film thickness using time only. There is no requirement for feedback using quartz crystal monitoring.

We present a comprehensive analysis of the micro-structural and optical properties of the CdS films as a function of argon gas flows, power, temperature, and deposition time. The CdS films deposited by pulsed DC sputtering were uniform, columnar and smooth and in all cases the films were stoichiometric and this was unaffected by gas flow, deposition power or temperature. All the films were in the preferred hexagonal structure even at room temperature. The films exhibited a high level of texture in the <111> direction. The grain size was typically ~50 nm. Pinholes and voids could be avoided by reducing the working gas pressure using gas flows below 20 sccm.

The mapping of the refractive index showed that the deposited CdS thin films were very uniform to ±0.8%. The band gap was measured to be 2.31 eV while refractive index (n) was measured to be 2.52 +/− 0.02. Increase in the gas flow leads to a reduction in the refractive index, while increasing the deposition power resulted in an increase of the refractive index. Pulsed DC magnetron sputtering allows close control of the thickness by changing the gas flows, deposition power and deposition temperature. With the increase of the substrate temperature up to 400 °C, the morphology of the thin film changes, leading to a more compact layer.

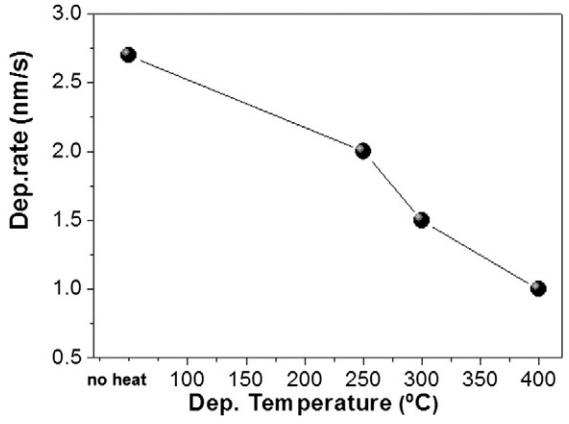

Fig. 13. Deposition rate as a function of deposition Temperature. The first point on the x-axis represents the deposition processed without heating.

The deposition rate achieved using pulsed DC magnetron sputtering is of particular note. Using 1500 W of deposition power at the magnetron target (corresponding to a power density of ~8.5 W m^{-2}) at 150 kHz pulsing frequency and 10 sccm argon gas flows, the deposition rate was measured to be 1.33 nm/s. However, this rate is achieved on a 5 cm × 5 cm substrate located on a 180 mm diameter rotating carrier. In this configuration, the substrate is exposed to the deposition flux only for a fraction or each revolution. The equivalent deposition rate for a static substrate is 8.66 nm/s, which is high and much faster than can be achieved using a chemical bath deposition or RF magnetron sputtering. As an example, the typical thickness of the CdS window layer in a thin film CdTe device is ~100 nm and this could be deposited in less than 12 s. We will investigate the properties of these thin layers in devices in future work. The high deposition rate makes the process highly attractive for industrial scale-up. Although target utilisation is poor with the planar magnetrons used in this study, this limitation could be overcome in a manufacturing environment by using rotating magnetrons.

Acknowledgements

The authors are grateful to the Engineering and Physical Science Research Council (EPSRC)(EP/J017361/1) for financial assistance under the Supergen SuperSolar Hub. They are also grateful to the Technology Strategy Board.

References

[1] A.D. Compaan, A. Gupta, J. Drayton, S.-H. Lee, S. Wang, 14% sputtered thin-film solar cells based on CdTe, Phys. Status Solidi B 241 (2004) 779.
[2] P. Jackson, D. Hariskos, E. Lotter, S. Paetel, R. Wuerz, R. Menner, et al., New world record efficiency for Cu (In, Ga) Se 2 thin-film solar cells beyond 20%, Prog. Photovolt. Res. Appl. 19 (2011) 894.
[3] K. Senthil, D. Mangalaraj, S. Narayandass, S. Adachi, Optical constants of vacuum-evaporated cadmium sulphide thin films measured by spectroscopic ellipsometry, Mater. Sci. Eng. B 78 (2000) 53.
[4] K. Assali, M. Boustani, A. Khiara, T. Bekkay, A. Outzourhit, E.L. Ameziane, et al., Some structural and optical properties of CdS thin films prepared by RF sputtering, Phys. Status Solidi A 178 (2000) 701.
[5] Z.R. Khan, M. Zulfequar, M.S. Khan, Optical and structural properties of thermally evaporated cadmium sulphide thin films on silicon (100) wafers, Mater. Sci. Eng. B 174 (2010) 145.
[6] U. Pal, R. Silva-Gonzalez, Optical characterization of vacuum evaporated cadmium sulfide films, Thin Solid Films 305 (1997) 345.
[7] E.B. Yous, T. Asikainen, V. Pietu, P. Cowache, M. Powalla, D. Lincot, Cadmium-free buffer layers deposited by atomic later epitaxy for copper indium diselenide solar cells, 3622000. 183.
[8] I. Repins, M.A. Contreras, B. Egaas, C. Dehart, J. Scharf, C.L. Perkins, 19.9%-efficient ZnO/CdS/CuInGaSe 2 solar cell with 81.2% fill factor z, 2008. 235.
[9] J. Rousset, F. Donsanti, P. Genevée, G. Renou, D. Lincot, High efficiency cadmium free Cu(In, Ga)Se2 thin film solar cells terminated by an electrodeposited front contact, Sol. Energy Mater. Sol. Cells 95 (2011) 1544.
[10] S. Spiering, D. Hariskos, M. Powalla, N. Naghavi, D. Lincot, CD-free Cu(In, Ga)Se2 thin-film solar modules with In2S3 buffer layer by ALCVD, Thin Solid Films 431–432 (2003) 359.
[11] B. Shin, O. Gunawan, Y. Zhu, N.A. Bojarczuk, S.J. Chey, S. Guha, Thin film solar cell with 8.4% power conversion efficiency using an earth-abundant Cu 2 ZnSnS 4 absorber, Prog. Photovolt. Res. Appl. 21 (2013) 72.
[12] S. Cinque, T. Unold, R. Klenk, S. Schorr, H. Schock, Cu 2 ZnSnS 4 thin film solar cells by fast coevaporation, Prog. Photovolt. Res. Appl. 19 (2011) 93.
[13] K.L. Earth, R.A. Enzenroth, W.S. Sampath, Advances in continuous, in-line processing of stable CdSlCdTe devices, Photovoltaic Specialists Conference, 2002, Conference Record of the Twenty-Ninth IEEE, 2002, p. 3.
[14] P.V. Meyers, Design of a thin film CdTe solar cell, Sol. Cells 23 (1988) 59.
[15] S. Duke, R.W. Miles, Characterisation of in-situ thermally evaporated CdS/CdTe thin film solar cells with Ni–P back contacts, J. Cryst. Growth 159 (1996) 916.
[16] R. Bube, CdTe junction phenomena, Sol. Cells 23 (1988) 1.
[17] R. Berrigan, N. Maung, S.J. Irvine, D. Cole-Hamilton, D. Ellis, Thin films of CdTe/CdS grown by MOCVD for photovoltaics, J. Cryst. Growth 195 (1998) 718.
[18] D.E. Swanson, R.M. Geisthardt, J.T. Mcgoffin, J.D. Williams, J.R. Sites, Improved CdTe solar-cell performance by plasma cleaning the TCO layer, IEEE J. Photovolt. 3 (2013) 838.
[19] A. Bosio, D. Menossi, S. Mazzamuto, N. Romeo, Manufacturing of CdTe thin film photovoltaic modules, Thin Solid Films 519 (2011) 7522.
[20] J.D. Major, Y.Y. Proskuryakov, K. Durose, Impact of CdTe Surface Composition on Doping and Device Performance in Close Space Sublimation Deposited CdTe, Solar Cells, 2013. 436.

[21] A. Ashour, N. El-Kadry, S.A. Mahmoud, On the electrical and optical properties of CdS films thermally deposited by a modified source, Thin Solid Films 269 (1995) 117.
[22] C.T. Tsai, D.S. Chuu, G.L. Chen, S.L. Yang, Studies of grain size effects in rf sputtered CdS thin films, J. Appl. Phys. 79 (1996) 9105.
[23] N.-H. Kim, S.-H. Ryu, H.-S. Noh, W.-S. Lee, Electrical and optical properties of sputter-deposited cadmium sulfide thin films optimized by annealing temperature, Mater. Sci. Semicond. Process. 15 (2012) 125.
[24] A. Gupta, A.D. Compaan, All-sputtered 14% CdS/CdTe thin-film solar cell with ZnO: Al transparent conducting oxide, Appl. Phys. Lett. 85 (2004) 684.
[25] J.K. Cooper, J. Cao, J.Z. Zhang, Exciton dynamics of CdS thin films produced by chemical bath deposition and DC pulse sputtering, ACS Appl. Mater. Interfaces 5 (2013) 7544.
[26] P. Kelly, R. Arnell, Magnetron sputtering: a review of recent developments and applications, Vacuum 56 (2000) 159.
[27] G. Bräuer, B. Szyszka, M. Vergöhl, R. Bandorf, Magnetron sputtering—milestones of 30 years, Vacuum 84 (2010) 1354.
[28] P.M. Kaminski, F. Lisco, J.M. Walls, Multilayer broadband antireflective coatings for more efficient thin film CdTe solar cells, IEEE J. Photovolt. 4 (2014) 452.
[29] F. Lisco, A. Abbas, B. Maniscalco, P.M. Kaminski, M. Losurdo, K. Bass, et al., Pinhole free thin film CdS deposited by chemical bath using a substrate reactive plasma treatment, J. Renew. Sustain. Energy 6 (2014) 011202.
[30] W. Petasch, B. Kegel, H. Schmid, K. Lendenmann, H. Keller, Low-pressure plasma cleaning: a process for precision cleaning applications, Surf. Coat. Technol. 97 (1997) 176.
[31] A. Rakhshani, Study of Urbach tail, bandgap energy and grain-boundary characteristics in CdS by modulated photocurrent spectroscopy, J. Phys. Condens. Matter 12 (2000) 4391.
[32] H. Fujiwara, Spectroscopic Ellipsometry Principles and Applications, 1st ed. Wiley, 2007.
[33] D.A. Mazón-Montijo, M. Sotelo-Lerma, L. Rodríguez-Fernández, L. Huerta, AFM, XPS and RBS studies of the growth process of CdS thin films on ITO/glass substrates deposited using an ammonia-free chemical process, Appl. Surf. Sci. 256 (2010) 4280.